CONF-840786--

PORTIONS OF THIS REPORT ARE ILLEGIBLE. It has been reproduced from the best available copy to permit the broadest possible availability.

ELECTRON SPECTROMETRY EXPERIMENTS WITH THE USE OF SYNCHROTRON RADIATION

Manfred O. Krause

Oak Ridge National Laboratory
Oak Ridge, Tennessee 37831

CONF-840786--3

DE85 001286

ABSTRACT

A survey of selected experiments is given to illustrate the recent advances that have been made in the study of the electronic structure and dynamics of free atoms.

Introduction

Within a very short period of time, synchrotron radiation has proven to be a powerful tool for probing and delineating the electronic structure and dynamics of atoms and, to no lesser degree, of molecules and solid matter.[1-3] This radiation source allows us to study the interaction of photons with the bound electrons as a continuous function of energy from less than 10 eV to more than 10 keV. In the simplest experiment, the photoabsorption experiment, the attenuation of the incoming photon beam by an ensemble of atoms or molecules is measured; in more detailed experiments, emission products are monitored, such as the fluorescence radiation, including x rays, the atomic or fragment ions, the Auger electrons and the photoelectrons. It is especially the analysis of the emitted electrons that has provided us with a detailed view of the structure and dynamics, and I shall restrict this presentation to studies by this type of technique, which may be labeled ESSR, electron spectrometry using synchrotron radiation. As much of the work done in previous years has already been summarized in various places,[3-5] only a small number of representative, recent studies will be discussed in detail.

Background

Two relations underlie the ESSR work: First, the energy balance of photoeffect

$$E_{Kin} = h\nu - E_B \qquad (1)$$

DISCLAIMER

This report was prepared as an account of work sponsored by an agency of the United States Government. Neither the United States Government nor any agency thereof, nor any of their employees, makes any warranty, express or implied, or assumes any legal liability or responsibility for the accuracy, completeness, or usefulness of any information, apparatus, product, or process disclosed, or represents that its use would not infringe privately owned rights. Reference herein to any specific commercial product, process, or service by trade name, trademark, manufacturer, or otherwise does not necessarily constitute or imply its endorsement, recommendation, or favoring by the United States Government or any agency thereof. The views and opinions of authors expressed herein do not necessarily state or reflect those of the United States Government or any agency thereof.

MASTER

DISTRIBUTION OF THIS DOCUMENT IS UNLIMITED

which identifies the level from which the photoelectron originates; and second, the transition probability of photoionization from a given ground state i

$$f_{fi} \propto \langle \Psi_f | \sum_{i=1}^{N} \vec{\alpha}_i \hat{\epsilon}\, e^{i\vec{k}\vec{r}_i} | \Psi_i \rangle \quad . \tag{2}$$

If two-electron transitions occur, Eq. 1 can be suitably modified and the electronic levels involved can often be identified. In Eq. 2, Ψ_i represents the initial (ground) state wavefunction, Ψ_f the final wavefunction for the ion and the continuum electron, and the operator contains the Dirac matrix $\vec{\alpha}_i$, the polarization $\hat{\epsilon}$ of the photon, and a term related to the multipolarity of the photon field. In the dipole approximation the operator reduces to r (in the length formulation):

$$f_{fi} \propto \int \Psi_f r \Psi_i dr = R \quad . \tag{3}$$

The goal is to find the best possible approximations to the "exact" wavefunction in the interplay between theory, which calculates f_{fi} in different models, and experiment, which measures one or more of the observables that are related to the matrix elements R and the phase shifts δ of the continuum waves. These observables are (1) the partial photoionization cross section σ, (2) the angular distribution parameter β which characterizes the angular dependence of the outgoing photoelectron, (3) the spin polarization parameter ξ which describes the photoelectron spin polarization perpendicular to the reaction plane, (4) the total spin transfer A from circularly polarized radiation to the photoelectron, and (5) the differential or angle dependent spin polarization transfer parameter α. These five parameters are sufficient for a "complete" description of the single electron photoionization process in a closed shell atom. In this case, three matrix elements and two phase differences are associated with the transitions allowed by the selection rules $\Delta j = 0, \pm 1$. The measurement of all five parameters, which requires the use of circularly polarized light in addition to linearly or unpolarized light, is a formidable task, but is a rewarding task for it allows the experimental determination of matrix elements and phase shifts. The first pioneering study of this nature has been carried out for the 5p electrons of Xe.[6] Similar measurements for other subshells and other closed shell atoms will be facilitated once more powerful synchrotron radiation sources will have become available. Up to the present, most experiments are directed at the determination of σ and β. Although this situation is not as satisfying as a "complete experiment," the determination of σ and β is sufficiently specific to help advance our knowledge of the electronic structure and dynamics.

Experimental Approach

The actual experimental procedure is based on the relation:

$$I_e \propto \frac{d\sigma}{d\Omega} = \frac{\sigma}{4\pi}\left[1 + \frac{\beta}{4}(1 + 3p\cos 2\phi)\right] \qquad (4)$$

which correlates the electron flux detected at the angle ϕ, defined relative to the major electric vector $\vec{E}_{//}$ of the linearly (actually elliptically) polarized light from the synchrotron radiation source, to the differential cross section, the partial cross section σ and the parameter β. Thus if for a given polarization p an angle ϕ is chosen so that $1 + 3p\cos 2\phi = 0$, the partial cross section σ is obtained directly on a relative basis or, following an appropriate calibration procedure, on an absolute basis. Similarly, β can be obtained from measurements at two angles using known polarization factors p. By relying on Eq. 4 as a basis for the experiment, we analyze the data in terms of the dipole approximation. The neglect of higher multipoles that may lead to a skewed angular distribution is, however, not serious at the low photon energies employed so far in most of the ESSR work.

A typical experimental setup, as the one used by the ORNL group, is shown in Fig. 1. Electrons originating from the source of free at.s or molecules are analyzed simultaneously in two spherical sector plate electrostatic spectrometers. Strong differential pumping allows a gas pressure of 10^{-2}Pa to be maintained in the source while the pressure in the monochromator remains at $10^{-7}$to 10^{-8}Pa. An oven operated at a temperature that produces a pressure of 10°to 10^{-1}Pa inside the oven provides a quasi-atomic beam along the axis of the photon beam. The resolution $\Delta E/E$=1% of the analyzers is commensurate with the bandpass of many monochromators presently in use.[1,2] Transitions from the various electronic levels can generally be distinguished, and sometimes also those involving term levels and vibrational levels.

For the mapping of σ and β over a given photon energy range, two approaches are at our disposal. In the first approach, we cut through the subshell structure by recording photoelectron spectra (PES) at fixed photon energies. As seen from Fig. 2, a PES spectrum identifies the photoionization processes, both single and double, from the available subshells and gives their relative probabilities and angular dependences. In the second approach, we follow the photoelectron intensity originating from a given level continuously as a function of photon energy. This approach which correlates the resulting σ and β data with a given or constant ionic state (CIS) is especially advantageous for the close study of resonance structures. An example is given in Fig. 3 which shows the

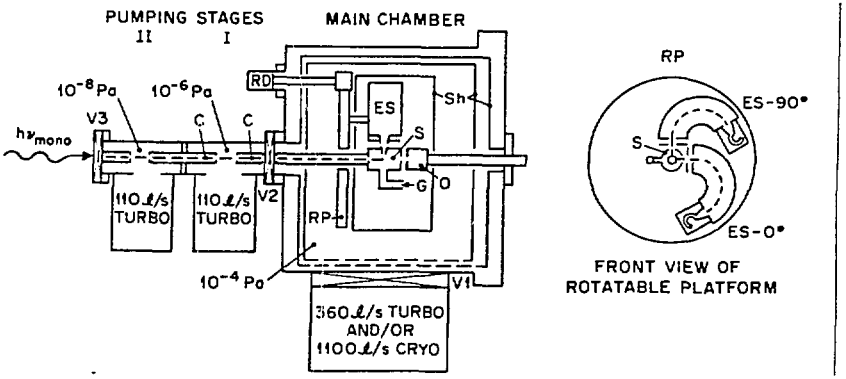

Fig. 1. Schematic of the ORNL electron spectrometer used for gas phase studies with the use of synchrotron radiation.

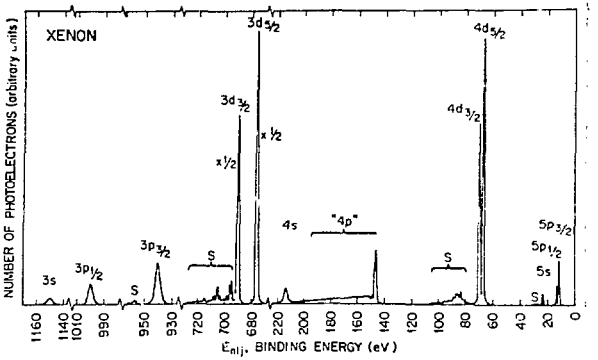

Fig. 2. Typical PES spectrum at fixed photon energy. Such spectra allow the determination of partial photoionization cross sections and photoelectron angular distribution parameters.

variation of the Xe $5p_{3/2}$ signal below the $5p_{1/2}$ threshold in the region of the autoionizing $5p_{1/2} \rightarrow$ ns, nd Rydberg series. Both approaches complement each other and it depends entirely on the problem at hand which approach should be emphasized.

The Partial Cross Section and β Parameter in Closed Shell Atoms

A basic question pertains to our knowledge and understanding of the dynamic behavior of the electrons in the various subshells, s, p, d and f, of closed shell atoms. In the case of the rare-gas atoms, extensive sets of data for both σ and β have been measured, and theoretical models have been developed that include relativistic and many-electron effects. A good accord has been achieved between theory and experiment for the p and d subshells of these atoms.[7] However, it is important to ascertain that this agreement is not unique to the rare gases. The elements of the 2a and 2b groups, as well as Pd and Yb are available for further and more

extensive study of the various subshells, including the 4f subshell in Yb and Hg. All these elements with closed subshells can be investigated as free atoms without undue difficulties.

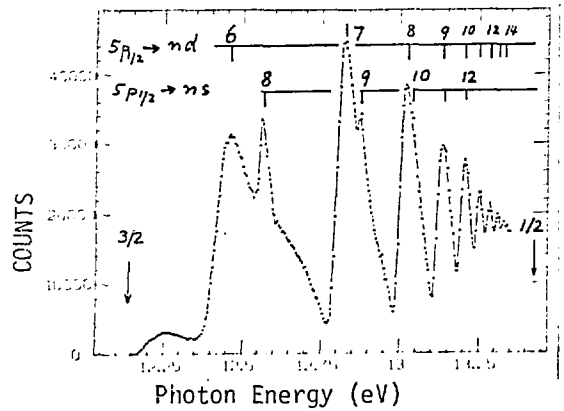

Fig. 3. The Xe $5p_{3/2}$ photoelectron intensity in the region of the $5p_{1/2}$ autoionization resonance series, as recorded.

The comparison made in Fig. 4 for the 5d electrons of Hg shows a reasonably good agreement between experiment[8] and theory.[9,10] The agreement extends over the entire range measured and includes the region of the Cooper minimum, which is especially sensitive to the quality of the wavefunctions chosen. Theory also represents the experimental data well for the 3d electrons of a lower Z element as seen in Fig. 5. Arguing that the difference between Pd, a closed shell atom accessible to theoretical treatment, and Ag, which has an additional electron (4s), should be small, the theoretical[11] β values of Pd are compared with the experimental data of Ag.[12] As for Hg and the rare gases, the comparison of data from free Ag atoms with atomic calculations is most stringent because of the absence of molecular and/or solid state effects. Interestingly enough, we do note in the case of Ag that the β values of the 3d electrons contained in the conduction band of metallic Ag are very close to the atomic values. This can then be regarded as one of the cases in which the atomic behavior remains dominant even in the bound state.

In contrast to the findings for the Hg 5d electrons, a large discrepancy between theory and experiment was reported[8] for the Hg 4f electrons.* A recent study of the Yb 4f subshell revealed no pronounced difference between theory and experiment for β and for the energy dependence of σ.[13,14] The preliminary results are shown in Fig. 6 and the comparison should be made above 40 eV, where no resonances interfere.

*Most recently, the authors (private communication) established as the cause for the discrepancy an unexpected and hitherto unknown energy dependence of the sodium salicylate detector used for photon flux calibration.

Taking the results for the p, d and f electrons of closed shell atoms *in toto*, we find the relativistic random phase approximation (RRPA) to be a very realistic model. However, for s electrons the RRPA or any other

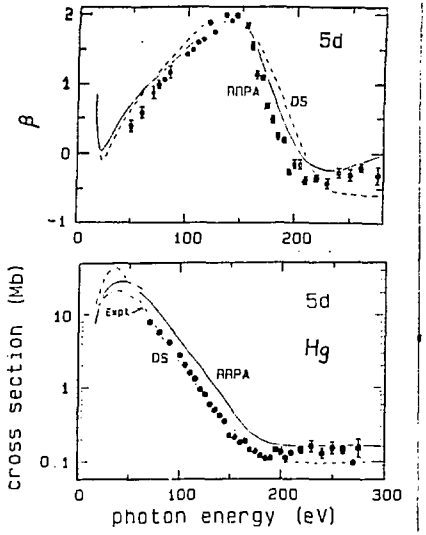

Fig. 4. The Hg 5d subshell properties: comparison of experiment[8] with theory in DS[9] and RRPA[10] models.

calculations are at variance with the observation.[15] This variance is amplified in the region of the Cooper minimum occurring near $h\nu$ = 35 eV for Xe 5s and Kr 4s. The question then arises as to which important interactions were not included in the theoretical model. In discussing the problem, we recognize the Xe 5s β parameters as a test case suitable to trace the evolution of atomic theory. The nonrelativistic single-particle model considers only the transition $5s \rightarrow \varepsilon p$ and hence predicts $\beta = 2$ at all photon energies. The relativistic treatment allows for the two transitions $5s \rightarrow \varepsilon p_{3/2}$ and $5s \rightarrow \varepsilon p_{1/2}$ which can interfere and lead to energy dependent β values, $\beta \leq 2$. The inclusion of many-electron interaction allows for the coupling of additional transitions (channels), such as $5p \rightarrow \varepsilon d$; εs and $4d \rightarrow \varepsilon f; \varepsilon p$ with the $5s \rightarrow \varepsilon p$ transition. This again leads to $\beta \leq 2$ values. The RRPA model that includes these channels and distinguishes the spin-orbit doublets predicts a sharp dip in β at the Cooper minimum, namely $\beta \cong 0$. However, recent experimental data (see e.g. Ref. 15) do not bear out this large excursion in β. Instead β drops only to about 1.4, indicating that the triplet channel, $^3P_1$, which causes the decrease is not as strong as predicted. An indication why the same model that predicts the properties of the p, d, and f electrons so well proved inadequate for describing the behavior of the s electrons has come from a recent experiment.[15] In that work it was established that the correlation

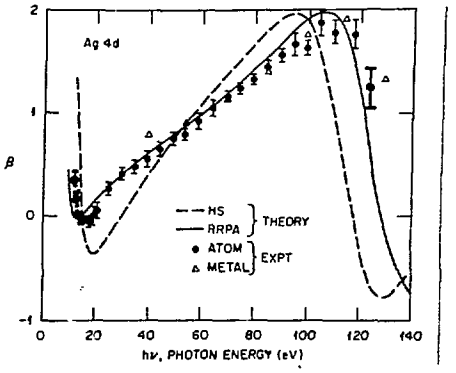

Fig. 5. The β parameter for Ag 4d electrons.[11,12] For σ, a similar accord exists between the RRPA theory and the experiment done with atomic Ag.

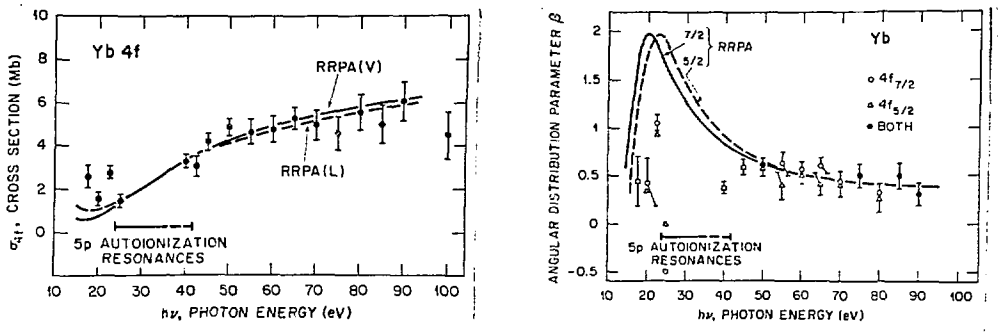

Fig. 6. The 4f dynamic parameters of atomic Yb.[13,14] The measured σ value is matched to theory at $h\nu$ = 40 eV. The excursions in the resonance region are omitted.

satellites are very intense throughout the Cooper minimum relative to the weak 5s → εp channels. As a result, even weak coupling between the two-electron excitation channels of the type $5p^2 \rightarrow n\ell$, $\varepsilon\ell'$ and 5s → εp could markedly affect the single-electron excitation channel. An analysis has been made to that effect,[16] but an explicit, quantitative calculation is still to be implemented to make this last step toward a "complete" model. In the meantime, it is interesting to note that a relativistic time-dependent local-density (RTDLD) calculation, which includes higher-order transitions *implicitly*, is in satisfactory accord with the data.[17] The strengths of the Xe 5s satellite lines within the Cooper minimum is shown in Fig. 7, and the status of the work on the Xe 5s β parameter is illustrated in Fig. 8, which shows the latest experimental and theoretical results.

In a different context, the behavior of correlation satellites has come into renewed focus owing largely to the availability of advanced instrumentation at synchrotron radiation sources. In these studies the intensity variation of the satellites above the thresholds of the Ar 1s and Ne 1s levels has been measured by way of the photoelectrons[18,19] or the Auger electrons,[20] in order to gain insight into the various mechanisms that lead to two-electron transitions.

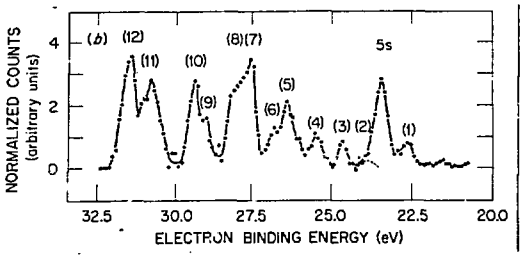

Fig. 7. PES spectrum of Xe at $h\nu$ = 33 eV in the Cooper minimum showing a large intensity of the correlation satellites compared with the 5s photoline intensity.[15]

Autoionization Resonances

Autoionization resonances have played a historic role in the use of synchrotron radiation.[21] Spectra similar to the Xe spectrum shown in Fig. 2 were recorded in absorption and on photographic plates. For the $np_{1/2}$ resonances of the rare gases, photoabsorption and photoelectron emission spectra are identical, because only one exit channel exists, namely the $\varepsilon p_{3/2}$ channel. However, for the next inner subshell, or in the case of openshell atoms with their multiplet structure, two or more exit channels are available, and the absorption and emission spectra are no longer identical. In fact, the PES emission spectra partition the total absorption spectrum into its components which are provided by the various exit channels. An example, the autoionization resonance in the region of

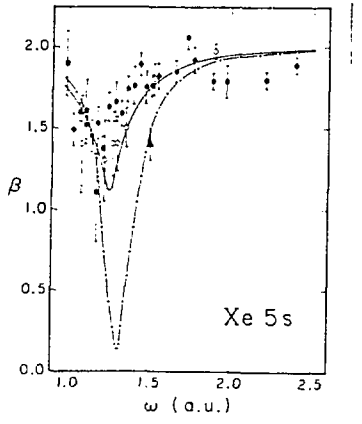

Fig. 8. The β parameter of the 5s subshell of Xe through the Cooper minimum. Experimental data are compared with theory. From Ref. 17.

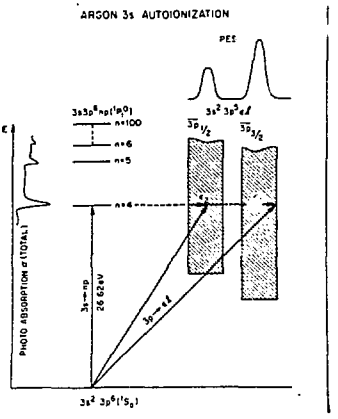

Fig. 9. Illustration of the autoionization process involving 3s excitation and 3p ionization in Ar. Note especially the relationship of σ(total) to the PES spectra that allow for the partition of σ(total) into its components.

the 3s → np excitation of Ar, is depicted schematically in Fig. 9, and the strength of the $3p_{3/2}$ → εd,εs channel is shown in Fig. 10. The spectrum of Fig. 10 as well as the corresponding β spectra for both spin-orbit components were recorded continuously by the CIS method,[22] while an earlier study[23] of the n = 4 resonance relied on a number of closely spaced PES spectra for identification.

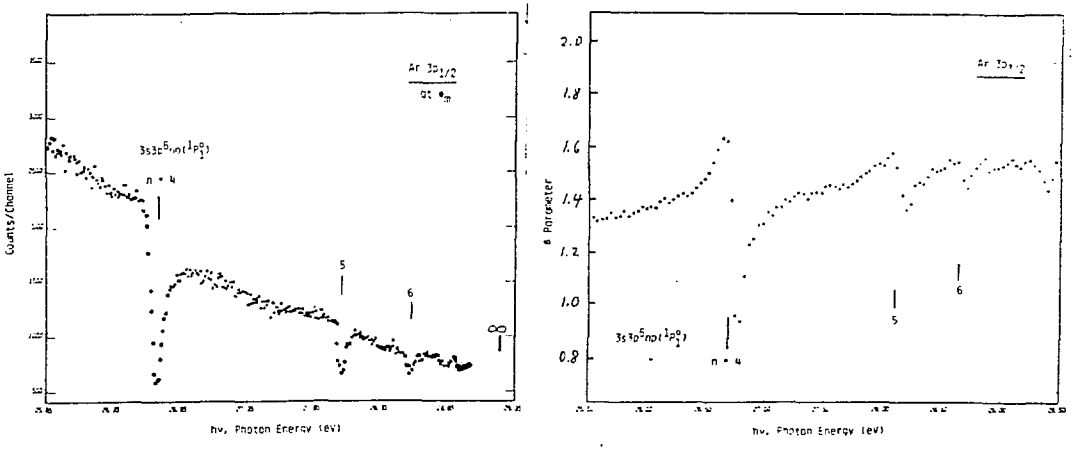

Fig. 10. Cross section and β parameter for the $^3P_{3/2}$ channel in the 3s autoionization region of Ar. The $^3P_{1/2}$ channel shows very similar trends.[22]

Resonance states converging to the $np_{1/2}$ limits of Ar, Kr and Xe have also been characterized by the spin polarization;[24,25] and RRPA predictions[26] of the spin parameters as well as the other dynamic parameters are in good agreement with experiment throughout the resonance region. A corresponding theoretical analysis of autoionization in the ns excitation region of the rare gases is, however, still to be undertaken.

Resonances in Openshell Atoms

The rare gases and other closed shell atoms have proven to be an excellent vehicle to advance our understanding of the electronic structure and dynamics of atoms. The knowledge of openshell atoms is less developed because of the greater complexity inherent in atoms with one or more partially filled shell. The resulting difficulties extend to both the experimental and the theoretical treatment. Autoionization resonances, which lead to pronounced effects in the rare gases as described above, give rise to spectacular phenomena in openshell atoms. This is because the transition strength to a partially filled subshell from another subshell with the same principal quantum number can be great and because many exit channels may be available due to the inherent multiplet structure. I shall present a few examples in the following.

Manganese: An excellent test case.

In 3d transition series elements, excitation of the type $3p \rightarrow 3d$ are possible and are expected to be strong. The excited states are embedded in the continua of the $3d \rightarrow \varepsilon f$; εp, the $4s \rightarrow \varepsilon p$ and two-electron channels, so that resonances in the various channels can arise. Resonances in absorption spectra were reported for these elements in the metallic state in one of the early applications of synchrotron radiation.[27] A detailed picture and analysis had to await, however, experiments done with free atoms. So far, atomic Cr,[28] Mn,[29-31] Fe,[32] Co[32] and Ni[32] have been investigated. Manganese having a half-filled 3d subshell is the simplest atom to be studied both experimentally and theoretically, and, indeed, three experimental and four theoretical studies have been reported in just the last two years. Figure 11 shows our σ and β results and theoretical

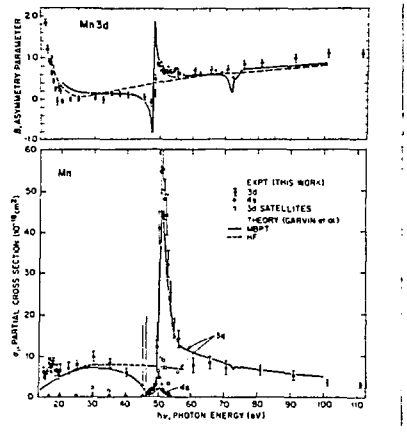

Fig. 11. The β parameter for the Mn 3d subshell, and σ for the various ionization channels observed between threshold and 110 eV, including the $3p \rightarrow 3d$ resonance region.[31]

results based on the independent-particle Hartree Fock (HF) model and the many-body perturbation theory (MBPT).[33] We note first that the HF calculation agrees satisfactorily with the data above 20 eV and outside the 3p resonance region, and second that the MBPT calculation, which couples the most important channels ($3p \rightarrow 3d$, $3d \rightarrow \varepsilon f$, $4s \rightarrow \varepsilon p$, etc.), agrees quite well with the data, both $\sigma(3d)$ and $\beta(3d)$, from 20 to 100 eV including the resonance region. This accord is the more remarkable as the comparison for σ is carried out on an absolute basis. In contrast to $\sigma(3d)$, the enhancement of $\sigma(4s)$ by the 3p resonance is underestimated by theory, indicating that further refinements are needed to achieve a full understanding of the interactions taking place. As seen from Fig. 11, the correlation satellites also experience an enhancement indicating a need to include the pertinent two-electron processes in the theoretical model. Such explicit considerations of two-electron processes are desirable not only to provide a basis for comparison with the experimental data on the satellites themselves but also to evaluate their effect on the single-electron channels, such as $4s \rightarrow \varepsilon p$. Although, on closer scrutiny, some shortcomings can be detected in both the experimental and theoretical studies, the overall agreement among the various works must be emphasized. The good agreement is especially gratifying since we are still at an early stage in our investigations of metal vapor atoms and open shell systems.

Lead: The missing adsorption series.

Lead is an excellent candidate for the study of a heavy element. It displays complex absorption and emission spectra due to multiplet and satellite structures and possesses many resonance states in the rather narrow energy region of $6s \rightarrow np$ and $5d \rightarrow np$, nf excitation. The open 6p subshell ($6p^2\ ^3P_0$ nominally) allows for strong transitions into the 6p level, but we shall be concerned here with the $6s \rightarrow 7p, 8p \ldots$ autoionization resonances, which have two open exit channels that leave the ion in either the $^2P_{3/2}$ state or the $^2P_{1/2}$ state. The special interest in this series comes from the fact that previous absorption spectra[34] showed lines only for the $6s \rightarrow np_{3/2}$ series. The question arises, which mechanisms could lead to the disappearance of the $np_{3/2}$ series. As illustrated in Fig. 12, an anomaly of this nature could occur

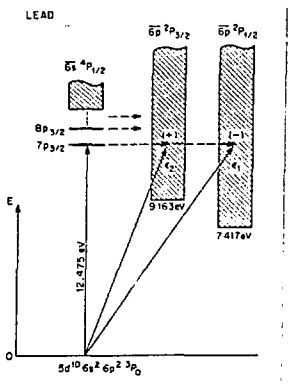

Fig. 12. Schematic of the 6s autoionization process in Pb with two observable exit channels.

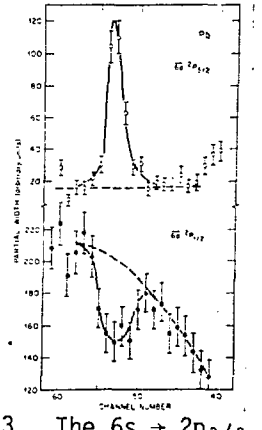

Fig. 13. The $6s \rightarrow 2p_{3/2}$ autoionization state, showing a Lorentzian and a window resonance of nearly equal magnitude in the two available exit channels.

if (a) excitation and deexcitation processes can no longer be separated, as for example in autoionization; (b) two (or more) exit channels are open; and (c) the various contributions cancel because of constructive interference in one channel and destructive interference in the other channel. Whether or not these criteria are met cannot be decided from an absorption measurement, which represents the sum of all contributions, but possibly from an ESSR emission experiment, which resolves the individual exit channels. This type of experiment pertains then to the initial state of the system, the neutral Pb atom $6s^26p^2\ ^3P_0$ plus the photon and the possible final states of the system, the residual ions $6s^26p\ ^2P_{3/2}$ and $6s^26p\ ^2P_{1/2}$ with the corresponding ejected photoelectrons. The theoretical treatment would have to consider the various routes, including the resonance states $6s^0\ 6p^2\ np_{3/2}\ ^4P_{1/2}$, to determine the probabilities for reaching the final states for the individual transition strengths and the interactions between the various channels, "excitation" and "deexcitation" (continuum exit) channels alike.

In a recent experiment,[35] the 6s → np resonance regions has been delineated by recording, for n = 7 through n = 11, the intensity variation of the photoelectrons corresponding to the two possible exit channels. The data show positive contributions in both channels for the $6s \rightarrow np_{1/2}$ states, but negative contributions in the $^2P_{1/2}$ channel and positive contributions in the $^2P_{3/2}$ channel for the $6s \rightarrow np_{3/2}$ states. In fact, the positive and negative contributions effectively cancel each other as seen from Fig. 13 in which the region of the $7p_{3/2}$ autoionization resonance is amplified. Accordingly, the $np_{3/2}$ states cannot be revealed in absorption, but can be seen and probed by measuring the final-state products, the photoelectrons.

Although we would not expect complete cancellation to occur in many systems, partial compensation will undoubtedly not be a rarity and would need to be considered as one of the possible causes for intensity anomalies in absorption spectra.

Experimental Identification of the Various Components in the K Auger Spectrum of N_2

An Auger spectrum contains lines of different origin depending upon the initial excitation state, single or multiple, and the final states reached. As a rule, these lines correspond to different categories which usually overlap with each other and cannot be separated in spectra obtained by the traditional electron, particle or x-ray excitation modes. Based on the analysis of the K Auger spectrum of N_2,[36] an experiment was described[37] several years ago in which the different categories of Auger lines could be separated under the selected excitation conditions that are feasible with the use of the tunable synchrotron radiation. Fig. 14 shows (a) the Auger spectrum produced by the customary excitation modes and by a white photon spectrum; (b) the normal or diagram spectrum which appears when the excitation energy lies between the K ionization edge and the first two-electron excitation state above the K edge; and (c) the spectrum that arises when the K electron is promoted to the first excited or resonance state πg, $2p\ ^1\Pi g$. In the last case, Auger lines appear in which the excited electron either participates in the transition, Aa, or remains

a spectator, As. The ESSR experiment has recently been performed[38] using the appropriate excitation energies, and the comparison of the observed Auger spectrum, Fig. 15, with the spectrum of Fig. 14 demonstrates that the various categories of Auger lines can, indeed, be differentiated and viewed separately.

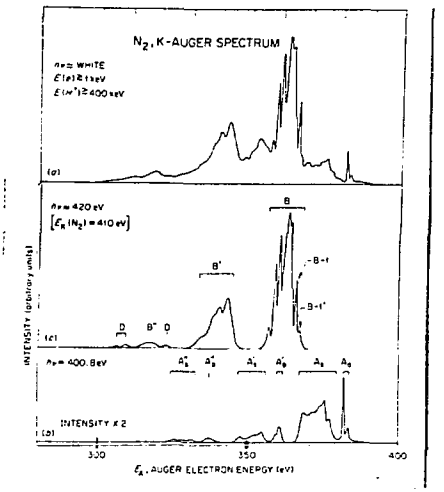

Fig. 14. The nitrogen K Auger spectrum excited in the normal mode (a), just above the K threshold (c), and at the resonance at 400.8 eV.[38] The spectra (b) and (c) are predicted.

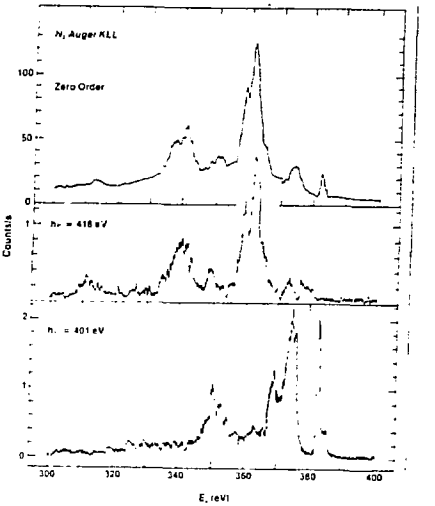

Fig. 15. The nitrogen K Auger spectra observed[38] in ESSR experiment under the conditions indicated in Fig. 14.

Atomic Effects in Free Molecules

The atomic character of the dynamic properties is often visible in the bound state. It can even be dominant if an orbital is localized. In Fig. 5 the atomic-like behavior of the 3d electrons in Ag metal was pointed out, and I now wish to give a few examples of atomic-like behavior of electrons in the valence orbitals of free molecules. The effect that may serve as a sensitive criterion is the Cooper minimum, which has been studied extensively in atoms. For example, the 3p wavefunction has a node resulting in a cross section minimum which occurs near 34 eV in Ar. A minimum is also observed in the β parameters, and in the regime of the dipole approximation, the β and σ minima occur at the same locus for a p electron. The behavior of the 3p electrons in elements adjacent to Ar is expected to be very similar to that observed in Ar, and the question arises to which extent the Cooper minimum will be manifested in the valence orbitals of molecules such as CCl_4, Cl_2, and HCl. In HCl the

similarity between the isoelectronic species Ar and Cl^- should be very close except for the changes that are introduced by the chemical environment. As an example,[39] Fig. 16 shows the PES spectrum of CCl_4 displaying three lone-pair orbitals with a predominant Cl 3p parentage and the bonding orbital $6t_2$. The β curves for these orbitals in the region where a Cooper minimum should occur are presented in Fig. 17. The lone-pair orbitals are seen to exhibit deep minima, nearly as pronounced as the minimum for Ar 3p, and even the bonding orbital displays a shallow dip. A theoretical analysis reveals that the minimum occurs for the εt_1 continuum channel. The presence of a minimum in the bonding orbital indicates that the atomic character of the Cl 3p wave function is not completely wiped out by the superposition with the C 2p wavefunction.

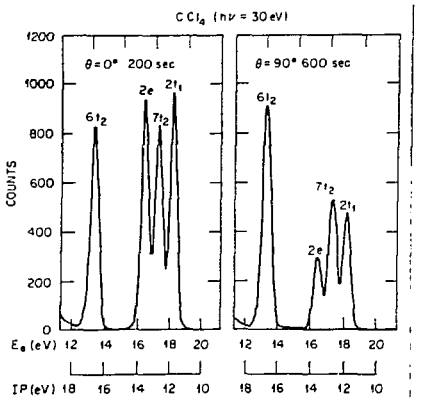

Fig. 16. PES spectrum of the valence orbitals of carbon tetrachloride.[39] According to Eq. 4, the angular distribution parameter β can be extracted from these recordings at two different angles.

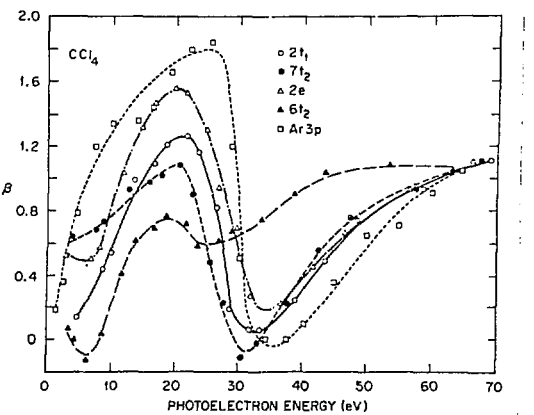

Fig. 17. The variation of β through the Cooper minimum for the molecular orbitals of CCl_4 and the atomic orbital of Ar 3p.[39]

The hydrogen halide series provides a view of the Cooper minimum in the bonding orbital 3σ and the lone-pair orbital 1π for electrons of 3p, 4p and 5p parentage.[40] In each case the 1π orbital exhibits a pronounced atomic-like dip, and the 3σ retains a shallow, broad minimum. This is shown for the β parameter in Fig. 18. The locus of the minimum for the lone-pair orbital through the series is plotted in Fig. 19 and compared

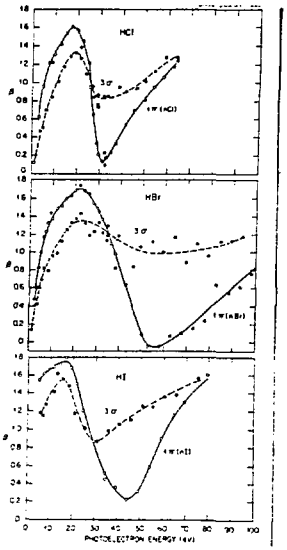

Fig. 18. The β parameter for the lone-pair orbital 1π and the bonding orbital 3σ in the hydrogen halide series.[40]

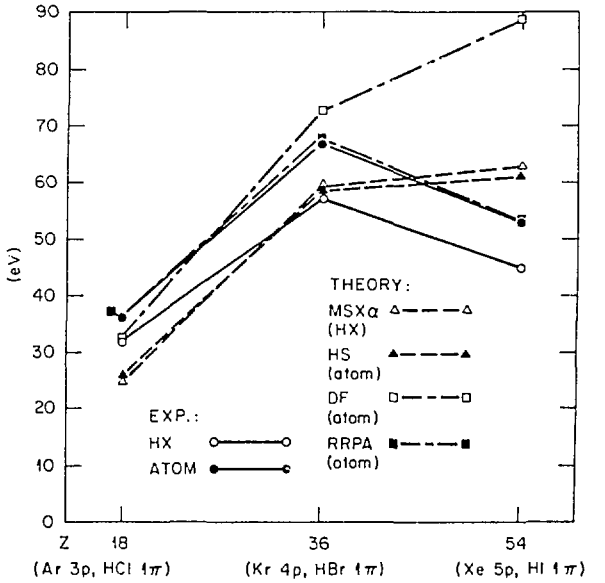

Fig. 19. The position of the minimum in σ and β for the rare gases and the isoelectronic halides in both theory and experiment.[40]

with the data on the rare gas atoms as well as with several theoretical models. The tracking of the molecular data with the atomic data is striking, emphasizing again the dominant atomic behavior in the molecular 1π orbitals. The comparison of theory with the atomic data on one hand and the molecular data on the other hand suggests that the extension of the multiple scattering $X\alpha$ model to include relativistic and many-electron effects would bring a similar accord with experiment for the molecular case as did the extension of the Hartree-Slater model for the atomic case.

Final Remarks

The number of experiments discussed in this presentation had to be necessarily limited, but hopefully the examples chosen will give a realistic picture of the advances that have been made in the study of the electronic structure and dynamics of free atoms. An important extension of the ESSR studies, which presently rely by and large on the determination of the partial cross section and the dipole angular distribution parameter, includes the determination of one or more spin polarization parameters. The feasibility and the power of such measurements have already been established.[41] The resonant Raman effect and the post-collision interactions occurring in the threshold regions have been described in several places.[4,5] Finally, it has been shown elsewhere[4,5] that the combination of laser excitation with synchrotron radiation allows the investigation of atoms in excited states.

Acknowledgements

Much of the work done by the ORNL group at the Synchrotron Radiation Center in Stoughton, Wisconsin involved the following individuals: T. A. Carlson, A. Svensson, A. Fahlman , F. Cerrina and F. A. Grimm. This work was sponsored by the Division of Chemical Sciences, Office of Basic Energy Sciences, U.S. Department of Energy under contract DE-AC05-840R21400 with the Martin Marietta Energy Systems, Inc.

References

1) *Synchrotron Radiation Research*, edited by H. Winick and S. Doniach, Plenum Press, New York (1980).

2) *Synchrotron Radiation, Techniques and Applications*, edited by C. Kunz, Springer Verlag, Berlin (1979).

3) B. Crasemann and F. Wuilleumier, Physics Today 37, 34 (June 1984).

4) *X-Ray and Atomic Inner-Shell Physics - 1982.* AIP Conference Proceedings Nr. 94 edited by B. Crasemann. American Institute of Physics, New York (1982). See articles by G. Wendin, O. Gunnarson and K. Schonhammer, F. P. Larkins, V. Schmidt, D. A. Shirley, et al, F. J. Wuilleumier, T. N. Chang and Y. S. Kim, and P. M. Koch.

5) F. Wuilleumier in *Atomic Physics* 7, edited by D. Kleppner, F. M. Pipkin, Plenum, New York (1981), p.491.

6) U. Heinzmann, J. Phys. B 13, 4367 (1980); 13, 4353 (1980).

7) W. R. Johnson and K. T. Cheng, Phys. Rev. A 20, 978 (1979).

8) P. H. Kobrin, P. A. Heimann, H. G. Kerkhoff, D. W. Lindle, C. M. Truesdale, T. A. Ferrett, U. Becker, and D. A. Shirley, Phys. Rev. A 27, 3031 (1983).

9) B. R. Tambe and S. T. Manson (unpublished results).

10) V. Radojevic and W. R. Johnson, Phys. Lett 92A, 75 (1982).

11) V. Radojevic and W. R. Johnson, J. Phys. B 16, 177 (1983).

12) M. O. Krause, et al. (to be published).

13) M. O. Krause, A. Svensson, T. A. Carlson and F. Cerrina (unpublished data).

14) V. Radojevic and W. R. Johnson (unpublished RRPA results).

15) A. Fahlman, M. O. Krause, T.A. Carlson and A. Svensson, Phys. Rev. A 30, 812 (1984). Related work cited therein.

16) G. Wendin and A. F. Starace, Phys. Rev. A 28, 3143 (1983).

17) F. A. Parpia, W.R. Johnson and V. Radojevic, Phys. Rev. A 29, 3173 (1984).

18) P. H. Kobrin, S. Southworth, C. M. Truesdale, D. W. Lindle, U. Becker and D. A. Shirley, Phys. Rev. A 29, 194 (1984).

19) P. A. Heimann, T.A. Ferrett, D. W. Lindle and D. A. Shirley, Abstract book of this conference, No. B2.

20) G. B. Armen, M. H. Chen, B. Crasemann, J. C. Levin, G. S. Brown and G. E. Ice, Abstract book of this conference. No. B2.

21) R. P. Madden and K. Codling, Phys. Rev. Lett 10, 516 (1963).

22) A. Svensson, M. O. Krause, T. A. Carlson and F. Cerrina (unpublished data).

23) K. Codling, J. B. West, A. C. Parr, J. L. Dehmer and R. L. Stockbauer, J. Phys. B 13, L693 (1980).

24) U. Heinzmann, F. Schäfers, K. Thimm, A. Wolcke and J. Wessler, J. Phys. B 12, L679 (1979).

25) F. Schäfers, G. Schönhense and U. Heinzmann, Phys. Rev. A 28, 802 (1983).

26) W. R. Johnson, K. T. Cheng, K. N. Huang and M. LeDourneuf, Phys. Rev. A 22, 989 (1980).

27) R. Haensel, C. Kunz, T. Sasaki and B. Sonntag, Appl. Optics 7, 301 (1968).

28) R. Bruhn, E. Schmidt, M. Schröder and B. Sonntag, J. Phys. B15, 2807 (1982).

29) R. Bruhn, E.Schmidt, H.Schröder and B. Sonntag, Phys. Lett 90A, 41 1982).

30) P. H. Kobrin, U. Becker, C. M. Truesdale, D. W. Lindle, H. G. Kerkhoff and D. A. Shirley (to be published).

31) M. O. Krause, T. A. Carlson and A. Fahlman, Phys. Rev. A 30 (Sept. 1984).

32) E. Schmidt, H.Schröder, B. Sonntag, H. Voss and H. E. Wetzel, J. Phys. B 16, 2961 (1983).

33) L. J. Garvin, E. R. Brown, S. L. Carter and H. P. Keely, J. Phys. B 16, 2961 (1983).

34) J. P. Connerade, W. R. S. Garton, M. W. D. Mansfield and M. A. P. Martin, Proc. Roy Soc. Loudon, Series A 357, 499 (1977).

35) M. O. Krause, F. Cerrina, A. Fahlman and T. A. Carlson, Phys. Rev. Lett 51, 2093 (1983).

36) See e.g. W. E. Moddeman, T. A. Carlson, M. O. Krause, B. P. Pullen, W. E. Bull and G. K. Schweitzer, J. Chem. Phys. 55, 2317 (1971).

37) M. O. Krause in *Proc. 24th Annual Conf. Mass Spectr. and Allied Topics*, edited by J. L. Margrave, Rice University, Houston (1976), p. 68.

38) W. Eberhardt, J. Stöhr, J. Feldhaus, E. W. Plummer and F. Sette, Phys. Rev. Lett 51, 2370 (1983).

39) T. A. Carlson, M. O. Krause, F. A. Grimm, P. Keller and J. W. Taylor, J. Chem. Phys. 77, 5340 (1982).

40) T. A. Carlson, A. Fahlman, M. O. Krause, T. A. Whitley and F. A. Grimm, J. Chem. Phys. (to be published).

41) Ch. Heckenkamp, F. Schäfers, G. Schönhense and U. Heinzmann, Phys. Rev. Lett 52, 421 (1984) and references therein.